Use of Piezoelectric Actuators as Elements of Intelligent Structures

Edward F. Crawley* and Javier de Luis†
Massachusetts Institute of Technology, Cambridge, Massachusetts

This work presents the analytic and experimental development of piezoelectric actuators as elements of intelligent structures, i.e., structures with highly distributed actuators, sensors, and processing networks. Static and dynamic analytic models are derived for segmented piezoelectric actuators that are either bonded to an elastic substructure or embedded in a laminated composite. These models lead to the ability to predict, a priori, the response of the structural member to a command voltage applied to the piezoelectric and give guidance as to the optimal location for actuator placement. A scaling analysis is performed to demonstrate that the effectiveness of piezoelectric actuators is independent of the size of the structure and to evaluate various piezoelectric materials based on their effectiveness in transmitting strain to the substructure. Three test specimens of cantilevered beams were constructed: an aluminum beam with surface-bonded actuators, a glass/epoxy beam with embedded actuators, and a graphite/epoxy beam with embedded actuators. The actuators were used to excite steady-state resonant vibrations in the cantilevered beams. The response of the specimens compared well with those predicted by the analytic models. Static tensile tests performed on glass/epoxy laminates indicated that the embedded actuator reduced the ultimate strength of the laminate by 20%, while not significantly affecting the global elastic modulus of the specimen.

Nomenclature

a = x coordinate of the center of the piezoelectric
b = width of the beam
B = modal damping of the beam
d_{31} = piezoelectric constant (strain/field)
$\mathcal{E}_{MAX}$ = maximum allowable piezoelectric field
$\bar{E}$ = modulus ratio of beam to piezoelectric
F = force applied at the ends of piezoelectric
F_1 = force applied at inner end of embedded piezoelectric
F_2 = force applied at outer end of embedded piezoelectric
$\bar{G}$ = modulus ratio of shear layer to piezoelectric
I_B = moment of inertia of beam
I_{EQ} = moment of inertia of beam plus embedded piezoelectric
$\bar{I}$ = nondimensional moment of inertia ($12 \cdot I_{EQ}/bt_B^3$)
K = modal stiffness of the beam
$\bar{K}$ = nondimensional modal stiffness of the beam
ℓ = length of the beam
L = length of the piezoelectric
m = half-length of the piezoelectric ($L/2$)
M = modal mass of the beam
M_K = lengthwise varying moment resultant
M_0 = moment applied by the piezoelectric
$\bar{t}_S$ = nondimensional bonding layer thickness
V = voltage applied across the piezoelectric
w = beam displacement in z direction
x = piezoelectric centered coordinate
$\bar{x}$ = nondimensional piezoelectric centered coordinate ($2x/L$)
z_M = z coordinate of midplane of embedded actuator
α = substructure equilibrium parameter
Γ = nondimensional shear transfer parameter
θ = thickness ratio (normalized by t_C)
λ_V = piezoelectric velocity feedback gain
Λ = piezoelectric strain ($d_{31}V/t_C$)
τ = applied shear stress
φ = mode shape
ψ = effective stiffness ratio

Subscripts

B = substructure
C = piezoelectric
S = shear layer
Z = embedded actuator

Superscripts

$(\tilde{\ })$ = normalization by beam length ℓ
$(\ )^s$ = surface of beam
$(\ )^+$ = right-hand end of actuator
$(\ )^-$ = left-hand end of actuator

Introduction

THE missions envisioned for large or precision space structures include a functional requirement for control of both rigid-body and elastic deformations. According to current thinking, this control will be exerted by a small number of high-authority actuators. This approach requires that the modes of the structure be known to a high degree of accuracy in order to provide high-authority control of the affected modes while avoiding spillover into the modes not modeled by the controller.[1] For large space structures, the dynamic behavior can be difficult to predict analytically and ground testing can be unreliable or unfeasible. These difficulties can lead to on-orbit open-loop behavior that differs substantially from preflight ground test measurements or analytic predictions.

An alternative to this approach is the use of an "intelligent structure," i.e., a structure with highly distributed actuator, sensor, and processor networks. Such a system would allow the use of software adjustments to modify and tune the closed-loop behavior via the distributed sensors and actuators. In addition, intelligent structures could enable the implementation of a number of flexible control strategies that cannot be used effectively with only a small number of sensors and actuators, including continuous,[2] hierarchical,[3] or wave[4] control algorithms. Within

Presented as Paper 86-0878 at the AIAA/ASME/ASCE/AHS 27th Structures, Structural Dynamics and Materials Conference, San Antonio, TX, May 19-21, 1986; received Aug. 6, 1986; revision submitted Jan. 1987.

*Associate Professor, Space Systems Laboratory, Department of Aeronautics and Astronautics. Member AIAA.

†Graduate Research Assistant, Space Systems Laboratory, Department of Aeronautics and Astronautics. Member AIAA.

the state of the art, the development of the distributed actuator network poses the greatest challenge. Since there must be a large number of actuators in such a distributed control system, it is desirable that they be compact, light, and simple, and that they not significantly modify the passive mechanical and dynamic properties of the system. Piezoelectric materials, which exhibit mechanical deformation when an electric field is applied, could be used for this purpose. Bonding or embedding segmented elements of these materials in a structure would allow the application of localized strains through which the deformation of the structural elements could be controlled. Due to their small size, a large number of piezoelectric actuator elements could be used without greatly increasing the mass of the structure.

Piezoelectrics have been employed extensively in a variety of transducers including strain gages, pressure transducers, and accelerometers. Lead zirconate titanate (PZT) piezoelectric ceramics have been used as actuators for structurally exciting turbomachinery[5] and other components[6] and for experimentally damping simple dynamic structures.[7] Recently, low-modulus piezoelectric film has been used both as an actuator[8] and a sensor.[9] However, comprehensive analytic models of piezoelectrics as actuators have not been developed.

In the first section of this paper, analytic models of the mechanical coupling of segmented piezoelectric actuators to the dynamics of the structural member will be developed, leading to the capability to predict, a priori, the motion of the structural member in response to a specified excitation voltage across the piezoelectric. In order to establish the fundamental elastic coupling of the piezoelectric/substructure system, static models of actuators coupled to structures are developed for a variety of actuator configurations, including both surface-bonded and embedded piezoelectrics. These coupling models can then be incorporated into any appropriate dynamic model of the substructure. As an example, the static models are coupled into a dynamic model of a Bernoulli-Euler cantilevered beam. In addition, a scaling analysis is performed on the segmented actuator that leads to a determination of how the effectiveness of the actuator changes with the scale of the structure and to the ability to rank the various piezoelectric materials in terms of their effectiveness as actuators.

In the second section of this paper, these theoretical models are experimentally verified. First, the laboratory feasibility of such a distributed actuator concept is established by successfully manufacturing specimens with surface-bonded and embedded actuators. Various specimens with distributed segmented piezoelectric actuators were tested and their measured responses were compared to those predicted by the analytic models. These specimens consisted of an aluminum beam with surface-bonded actuators and two composite beams with embedded actuators. Initially, a glass/epoxy material was used in the manufacture of the composite beam in order to avoid the problem of electrically shorting the piezoelectrics. Subsequently, a manufacturing technique was developed that allowed the piezoelectrics to be embedded inside a graphite/epoxy laminate without electrically shorting the actuators through the graphite fibers and a graphite/epoxy beam with embedded actuators was manufactured and tested. Static tests were also performed on a number of glass/epoxy laminates with embedded piezoelectrics in order to determine the effect of the actuator on the passive structural stiffness and strength of the laminate.

Static Model of Piezoelectric/Substructural Coupling

In this section, static elastic models for surface-bonded and embedded segmented actuators exciting extension and bending in the substructure will be presented. For the surface-bonded cases, two solutions will be derived. In the first, an elastic bonding layer of a finite thickness will be assumed to be present between the piezoelectric and the substructure, leading to a classic shear lag solution. When the shear lag in the bonding layer goes to zero, this solution will be shown to reduce to a simpler model—that of a perfectly bonded piezoelectric. For the embedded cases, only the simple, perfectly bonded model will be derived, since it will be assumed that the interlaminar bonding layer between the actuators and the surrounding material is sufficiently thin that neglecting the shear layer will not introduce any significant errors into the model.

Surface Bonded Actuators

Formulation for Finite Bonding Layer

In Fig. 1, two piezoelectric elements are shown bonded by a finite-thickness bonding layer to an elastic substructure. The arrow in the figure indicates the direction of the electric field that will cause the piezoelectric to expand. If an electric field is applied across both piezoelectrics in the direction of the arrows, the substructure will be deformed in extension. If the field is applied across one piezoelectric in the direction of the arrow and reversed on the second, the substructure will be deformed in bending.

In order to derive the governing equations, the equilibrium of the differential element $\mathcal{A}$ outlined by the dashed area in Fig. 1 will be examined. Under the assumption of pure one-dimensional shear in the bonding layer and pure extensional strain in the piezoelectric and substructure, the strain-displacement relationships are

$$\epsilon_C = \frac{du_C}{dx} = u_C' \tag{1}$$

$$\epsilon_B^s = \frac{du_B}{dx} = u_B^{s\prime} \tag{2}$$

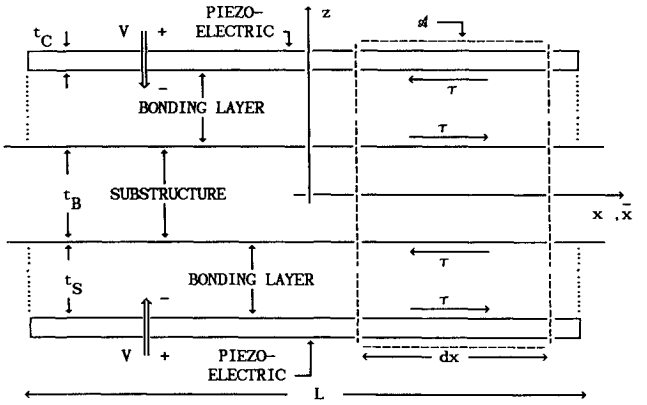

Fig. 1 Geometry of piezoelectrics bonded to an elastic substructure through a finite thickness bonding layer.

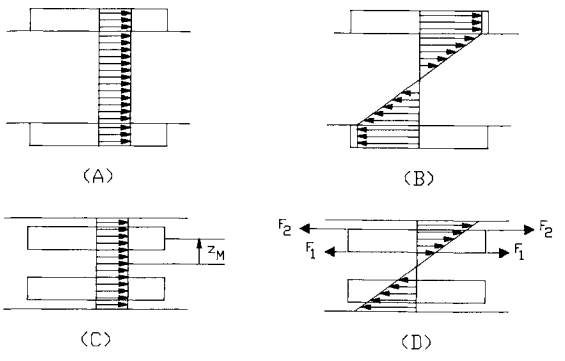

Fig. 2 Assumed piezoelectric-substructure strain distributions: a) surface-bonded extension, $\alpha = 2$; b) surface-bonded bending, $\alpha = 6$; c) embedded extension; d) embedded bending.

$$\gamma = \frac{u_C - u_B^s}{t_S} \tag{3}$$

If the piezoelectrics excite bending in the substructure, a linearly varying Bernoulli-Euler strain distribution will be assumed in the beam (Fig. 2b); if they excite extension, a uniform strain distribution will be assumed (Fig. 2a). In either case, the stress-free ends of the segmented actuator cause the piezoelectric to have a uniform strain through its thickness (Figs. 2a and 2b). With these assumptions, the equilibrium equations for the area $\mathfrak{A}$ are

$$\frac{d\sigma_C}{dx} - \frac{\tau}{t_C} = 0 \tag{4}$$

$$\frac{d\sigma_B^s}{dx} + \frac{\alpha\tau}{t_B} = 0 \tag{5}$$

where α is the constant depending on the assumed beam strain distribution. For a linear Bernoulli-Euler strain distribution, $\alpha = 6$ (Fig. 2b); for a uniform extensional strain, $\alpha = 2$ (Fig. 2a). In both Eqs. (2) and (5), the superscript s refers to the strain and stress quantity on the surface of the beam.

The stress-strain relationship for the piezoelectric is similar to that of a thermoelastic material,[10] the thermal strain term being replaced by the piezoelectric strain term $d_{31}V/t_C \equiv \Lambda$, giving

$$\sigma_C = E_C\left(\epsilon_C - \frac{d_{31}V}{t_C}\right) = E_C(\epsilon_C - \Lambda) \tag{6}$$

The term d_{31} is the piezoelectric constant relating the electric field applied across the piezoelectric to the resulting strain. For the beam and bonding layer, the isotropic stress-strain relations are

$$\sigma_B^s = E_B\epsilon_B^s \tag{7}$$

$$\tau = G\gamma \tag{8}$$

Solution for Finite Bonding Layer

Equations (1-8) are the eight governing equations in the eight unknowns: the stresses and strains in the piezoelectric, the substructure, and the bonding layer (σ_C, σ_B^s, τ, ϵ_C, ϵ_B^s, γ) and the displacements in the piezoelectric and the substructure (u_C and u_B^s). Substituting Eq. (3) into Eq. (8), inserting the result into Eqs. (4) and (5), and differentiating and substituting Eqs. (1), (2), (6), and (7) yield two coupled second-order differential equations that can be further reduced to a pair of uncoupled fourth-order differential equations,

$$\epsilon_B^{s\,iv} - \Gamma^2\epsilon_B^{s\,\prime\prime} = 0 \tag{9}$$

$$\epsilon_C^{\,iv} - \Gamma^2\epsilon_C^{s\,\prime\prime} = 0 \tag{10}$$

where differentiation is with respect to the nondimensional coordinate $\bar{x}$ and the shear lag parameter and the beam to piezoelectric stiffness ratio are

$$\Gamma^2 = \frac{\bar{G}\theta_S}{\bar{t}_S^2}\left(\frac{\psi+\alpha}{\psi}\right) \tag{11}$$

$$\psi = \frac{E_B t_B}{E_C t_C} = \bar{E}\theta_B \tag{12}$$

Although the fourth-order equations [(9) and (10)] appear uncoupled, their solutions are, in fact, coupled by the underlying second-order equations. Solving Eqs. (9) and (10) for the strain distributions in the piezoelectric and substructure and applying these coupling constraints give

$$\begin{bmatrix} \epsilon_C \\ \epsilon_B^s \end{bmatrix} = \begin{bmatrix} 1 \\ 1 \end{bmatrix} B_1 + \begin{bmatrix} 1 \\ 1 \end{bmatrix} B_2\bar{x} + \begin{bmatrix} \dfrac{\psi}{\alpha} \\ 1 \end{bmatrix} B_3 \sinh\Gamma\bar{x} + \begin{bmatrix} \dfrac{-\psi}{\alpha} \\ 1 \end{bmatrix} B_4 \cosh\Gamma\bar{x} \tag{13}$$

The four strain boundary conditions can now be applied to determine the four unknown constants. It should be noted that the piezoelectric strain term Λ does not appear explicitly in Eq. (13), but will enter into the solution through the boundary conditions. A segmented piezoelectric actuator bonded to the surface of a substructure will have stress-free ends, implying that at its ends ϵ_C must equal the piezoelectric strain term Λ [Eq. (6)]. The points on the substructure underlying the ends of the actuator may have an arbitrary nonzero strain due to loading or deformations other than those caused by the action of the piezoelectric. With these assumptions, the boundary conditions are, at

$$\bar{x} = +1: \quad \epsilon_C = \Lambda, \qquad \epsilon_B^s = \epsilon_B^{s+}$$

and at

$$\bar{x} = -1: \quad \epsilon_C = \Lambda, \qquad \epsilon_B^s = \epsilon_B^{s-}$$

where ϵ_B^{s+} and ϵ_B^{s-} are the known substructure strain values at the locations of the left (−) and right (+) ends of the piezoelectric segment.

Substituting these boundary conditions into Eq. (13), the unknown constants are found to be

$$B_1 = \frac{\psi}{\psi+\alpha}\left(\frac{\epsilon_B^{s+} + \epsilon_B^{s-}}{2} + \frac{\alpha\Lambda}{\psi}\right) \tag{14a}$$

$$B_2 = \frac{\psi}{\psi+\alpha}\left(\frac{\epsilon_B^{s+} - \epsilon_B^{s-}}{2}\right) \tag{14b}$$

$$B_3 = \frac{\alpha}{(\psi+\alpha)\sinh\Gamma}\left(\frac{\epsilon_B^{s+} - \epsilon_B^{s-}}{2}\right) \tag{14c}$$

$$B_4 = \frac{\alpha}{(\psi+\alpha)\cosh\Gamma}\left(\frac{\epsilon_B^{s+} + \epsilon_B^{s-}}{2} - \Lambda\right) \tag{14d}$$

To facilitate the later incorporation of these static coupling models into the dynamic model of the substructure, it is desirable to have an explicit expression for the force applied by the piezoelectric on the substructure. In this case, the shear stress τ in the bonding layer is derived by substituting Eqs. (13) and (14) into Eqs. (1) and (2) to obtain expressions for u_C' and $u_B^s{}'$. After integrating and substituting into Eq. (3), the result is inserted into Eq. (8), yielding

$$\frac{\tau}{E_B} = \frac{\bar{G}}{\bar{t}_S\bar{E}\Gamma}\left[\frac{\epsilon_B^{s+} - \epsilon_B^{s-}}{2}\frac{\cosh\Gamma\bar{x}}{\sinh\Gamma} + \left(\frac{\epsilon_B^{s+} + \epsilon_B^{s-}}{2} - \Lambda\right)\frac{\sinh\Gamma\bar{x}}{\cosh\Gamma}\right] \tag{15}$$

The complete solution for the strains in the piezoelectric and the substructure along with the solution for the stress in the bonding layer has now been determined. The strains [Eqs. (13) and (14)] and stresses [Eq. (15)] can be seen to depend on the strains in the substructure at the boundaries (ϵ_B^{s+} and ϵ_B^{s-}) and the voltage applied to the piezoelectric $\Lambda = d_{31}V/t_C$. The terms dependent on ϵ_B^{s+} and ϵ_B^{s-} are merely

the representation of the additional passive stiffness added by bonding a reinforcement to the surface and can be correctly modeled in a conventional analysis. The new effect, the ability to strain or apply stress to the substructure actively, is represented by the terms dependent on Λ. In order to illustrate these terms more explicitly, the applied strain boundary conditions on the end of the substructure (ϵ_B^{s+} and ϵ_B^{s-}) can be set to zero, and Eqs. (13) and (15) reduce to

$$\begin{bmatrix} \frac{\epsilon_C}{\Lambda} \\ \frac{\epsilon_B^s}{\Lambda} \end{bmatrix} = \begin{bmatrix} 1 \\ 1 \end{bmatrix} \frac{\alpha}{\psi+\alpha} - \begin{bmatrix} \frac{-\psi}{\alpha} \\ 1 \end{bmatrix} \frac{\alpha}{(\psi+\alpha)\cosh\Gamma} \cosh\Gamma\bar{x} \tag{16}$$

$$\frac{\tau}{E_B} = \frac{-\bar{G}}{t_S\bar{E}\Gamma}\left(\frac{\sinh\Gamma\bar{x}}{\cosh\Gamma}\right)\Lambda \tag{17}$$

Equation (16) is plotted in Fig. 3 for various values of Γ and for $\psi = 14.5$ and $\alpha = 6$, typical for a piezoelectric ceramic exciting bending in an aluminum bar 10 times its thickness. The Γ parameter [Eq. (11)] is the nondimensional shear lag parameter that indicates the effectiveness of the shear transfer. It is primarily influenced by the stiffness and thickness of the bonding layer. As the shear modulus G of the bonding layer increases or the thickness t_S decreases, Γ increases, the shear lag becomes less significant, and the shear is effectively transferred over a smaller zone close to the end of the piezoelectric.

The ψ parameter [Eq. (12)], which is equal to the product of the modulus and thickness ratios, sets the maximum fraction of the piezoelectric strain that can be induced in the substructure. This strain level will be achieved if the bond is perfect, i.e., Γ is infinite, and approached if Γ is large. As ψ approaches zero, the strain induced in the substructure will be equal to the piezoelectric strain Λ [Eq. (16)]. This is the case of a very compliant or thin substructure, as compared to the piezoelectric. Conversely, a large ψ, corresponding to a relatively thick, high-modulus substructure, implies that the strain induced in the substructure is small. Thus, the desirable parameters of a bonded piezoelectric actuator are large Γ (implying a good bond) and low ψ (implying a stiff actuator compared to the substructure).

Solution for Perfectly Bonded Actuator

A perfectly bonded actuator represents the limiting case of an infinitely stiff bonding layer, with the shear lag parameter

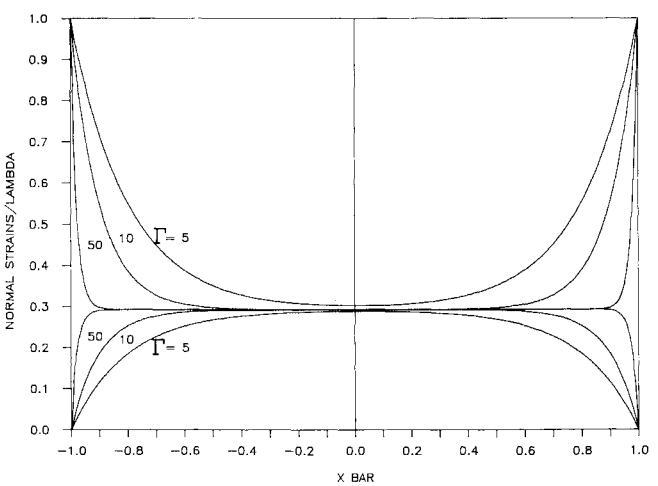

Fig. 3 Piezoelectric and substructure strains for various values of Γ.

Γ approaching infinity. In this case, a sharp rise in the shear stress exists at the ends of the piezoelectric, indicating that the strain is transferred between the piezoelectric and the substructure over an infinitesimal distance near the ends of the actuator. Under these idealized assumptions, Eqs. (13) and (14) reduce to

$$\epsilon_B = \epsilon_C = \frac{\psi}{\psi+\alpha}\left[\frac{\epsilon_B^{s+}+\epsilon_B^{s-}}{2} + \frac{\epsilon_B^{s+}-\epsilon_B^{s-}}{2}\bar{x}\right] + \frac{\alpha}{\psi+\alpha}\Lambda \tag{18}$$

The entire shear force is now effectively transferred at a concentrated point at the ends of the piezoelectric. This force, applied at $\bar{x} = \pm 1$, is

$$\frac{F}{E_B t_B b} = \frac{1}{(\psi+\alpha)}\left[\frac{\epsilon_B^{s+}+\epsilon_B^{s-}}{2} + \frac{\epsilon_B^{s+}-\epsilon_B^{s-}}{2}\bar{x}\right] - \left[\frac{1}{\psi+\alpha}\right]\Lambda \tag{19}$$

If bending is being excited, the moment applied to the beam by these forces is equal to

$$M_0 = Ft_B \tag{20}$$

Equations (18–20) for the perfectly bonded actuator can be obtained in either of two ways: by formally taking the limit of Eq. (13) as Γ approaches infinity or by directly equating the strains in the piezoelectric and the substructure [Eqs. (1) and (2)] and solving the equations of elasticity. This approximation is good for thinner, stiffer bonding layers. For values of Γ of 30 or greater, the strain energy induced in the substructure by the actuator is within 5% of the strain energy induced when the actuator is perfectly bonded. Therefore, for values of Γ greater than 30, the perfectly bonded solution will provide results sufficiently accurate for engineering models. For thicker, softer bonding layers, the complete shear lag solution [Eqs. (13) and (14)] must be used.

The analysis for the surface-bonded piezoelectric actuator exciting bending and extension in an elastic substructure is now complete. As noted previously, if both piezoelectrics in Fig. 1 have an applied voltage in the direction of the arrows shown, extension will be excited in the substructure and $\alpha = 2$. If the voltage on one is reversed, bending is excited and $\alpha = 6$. Note that, because of this higher value for α,

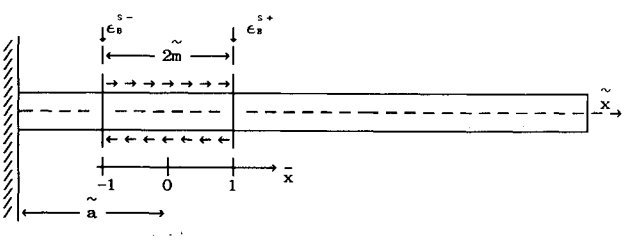

Fig. 4 Cantilevered beam under surface-localized shear loading.

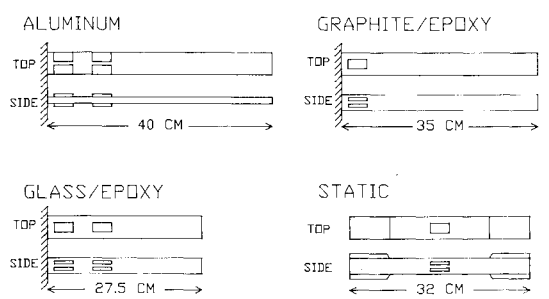

Fig. 5 Dynamic and static test specimens (side view not to scale).

piezoelectrics are more effective in exciting surface strain in bending than in extension. The results for the strains and forces induced by the actuator are summarized in Table 1 for all four cases.

Embedded Actuators

The case of perfectly bonded piezoelectric actuators embedded within a laminated substructure will now be presented. In current graphite/epoxy composite laminates,[11] the interlaminar bonding layer is on the order of 5 fiber diameters ($\simeq 1$ μm) and typical values of the shear lag parameter Γ for this thickness and typical epoxies are on the order of 1000. This is sufficiently large to allow the influence of the interlaminar bonding layer to be neglected. Therefore, it is assumed that the actuator is perfectly bonded to the surrounding laminate and that the strain in the actuator is compatible with the surrounding structure. Figures 2c and 2d show the geometry of the deformation of a pair of piezoelectric actuators embedded in such a substructure. As in the surface-bonded case, the actuators can excite either extension or bending, depending on the direction of the applied electric field. The resulting forces and strains for the bending case will be derived in detail, and the extensional case will then be summarized.

Embedded Actuators in Bending

In this analysis, both the actuators and the surrounding substructural laminate are assumed to be in Bernoulli-Euler bending about the neutral axis. This model differs from the surface-bonded case, in which the strain in the piezoelectric is compatible with the substructure only at its inner surface and is constant through the thickness of the piezoelectric (Fig. 2b). In this embedded case, the strain is now compatible at both the inner and outer surfaces and must therefore be linearly varying through the thickness of the piezoelectric (Fig. 2d). Under these assumptions, the equilibrium relations are

$$\sigma_B = \frac{M_0 z}{I_{EQ}} + \frac{M_K z}{I_{EQ}} \tag{21}$$

$$\sigma_C = \frac{6\Delta F}{bt_C^2}(z - z_M) + \frac{\bar{F}}{bt_C} \tag{22}$$

where M_K is a lengthwise varying moment due to loading or deformations other than those caused by the action of the piezoelectric and $\bar{F} = (F_1 + F_2)$ and $\Delta F = (F_1 - F_2)$ are the sum and difference, respectively, of the load applied at the concentrated points at the inner and outer ends of the piezoelectric (Fig. 2d). M_0 is the moment applied to the substructure by the piezoelectric at its ends and is equal to

$$M_0 = 2\left[\Delta F \frac{t_C}{2} + \bar{F} z_M\right] \tag{23}$$

Assuming that the laminate behaves like a beam with an effective flexural modulus E_B, the stress-strain relations are the same as those given in Eqs. (6) and (7). Equating the strains in the piezoelectric and substructure at $z = (z_M - t_C/2)$ for the inner surface and $z = (z_M + t_C/2)$ for the outer surface and substituting the stress-strain relationships [Eqs. (6) and (7)] and the equilibrium expressions [Eqs. (21-23)] gives a pair of equations for $\bar{F}$ and ΔF

$$\bar{F} = \frac{-12(M_K/t_C)\theta_Z}{24\theta_Z^2 + \psi\theta_B^2\bar{I} + 2} - \frac{2E_C t_C b + E_B t_B b\theta_B^2 \bar{I}}{24\theta_Z^2 + \psi\theta_B^2\bar{I} + 2}\Lambda \tag{24}$$

$$\Delta F = \frac{-2(M_K/t_C)}{24\theta_Z^2 + \psi\theta_B^2\bar{I} + 2} + \frac{4E_C t_C b\theta_z}{24\theta_Z^2 + \psi\theta_B^2\bar{I} + 2}\Lambda \tag{25}$$

These two equations can now be inserted back into the equilibrium relations and solved for the resulting strains.

In order to allow coupling of this embedded actuator model to that of the deformation of the substructure in a manner similar to the surface-bonded case, the lengthwise varying moment M_K is expessed as a linearly varying function of the strains ϵ_B^{s+} and ϵ_B^{s-} present on the surface of the beam at the ends of the piezoelectric

$$M_K = \frac{-I_{EQ}E_B}{t_B}(\epsilon_B^{s+} + \epsilon_B^{s-}) - \frac{I_{EQ}E_B}{t_B}(\epsilon_B^{s+} - \epsilon_B^{s-})\bar{x} \tag{26}$$

Inserting Eqs. (24-26) into the equilibrium equation for the beam [Eq. (21)] and substituting the stress-strain relationship [Eq. (7)], the strain in the acturator and in the surrounding material is

$$\epsilon_B = \epsilon_C = \frac{2\psi\theta_B\bar{I}(z/t_C)}{24\theta_z^2 + \psi\theta_B^2\bar{I} + 2}\left(\frac{\epsilon_B^{s+} + \epsilon_B^{s-}}{2} + \frac{\epsilon_B^{s+} - \epsilon_B^{s-}}{2}\bar{x}\right) + \frac{24\theta_Z(z/t_C)}{24\theta_Z^2 + \psi\theta_B^2\bar{I} + 2}\Lambda \tag{27}$$

The moment applied at the ends of the piezoelectric can be found by substituting Eqs. (24-26) into Eq. (23) to obtain

$$\frac{M_0}{E_B t_B^2 b} = \frac{(12\theta_Z^2 + 1)\bar{I}}{3(24\theta_Z^2 + \psi\theta_B^2\bar{I} + 2)}\left(\frac{\epsilon_B^{s+} + \epsilon_B^{s-}}{2} + \frac{\epsilon_B^{s+} - \epsilon_B^{s-}}{2}\bar{x}\right) - \frac{2\theta_Z\theta_B\bar{I}}{24\theta_Z^2 + \psi\theta_B^2\bar{I} + 2}\Lambda \tag{28}$$

The resulting expressions for the strains and moments are similar to those obtained for the surface-bonded cases, with terms dependent on the strain in the substructure at the boundaries and a term that is directly dependent on the voltage applied across the piezoelectric.

Embedded Actuators in Extension

A similar analysis can be performed for the case of piezoelectrics exciting extension in the surrounding elastic material. In this case, the resulting strains are

$$\epsilon_B = \epsilon_C = \frac{\bar{E}(\theta_B - 2)}{2 + \bar{E}(\theta_B - 2)}\left(\frac{\epsilon_B^{+} + \epsilon_B^{-}}{2} + \frac{\epsilon_B^{+} - \epsilon_B^{-}}{2}\bar{x}\right) + \frac{2}{2 + \bar{E}(\theta_B - 2)}\Lambda \tag{29}$$

and the force applied at each end of the piezoelectric is

$$\frac{F}{E_B t_B b} = \frac{-(\theta_B - 2)}{2\theta_B + \bar{E}(\theta_B - 2)\theta_B}\left(\frac{\epsilon_B^{+} + \epsilon_B^{-}}{2} + \frac{\epsilon_B^{+} - \epsilon_B^{-}}{2}\bar{x}\right) - \frac{(\theta_B - 2)}{2\theta_B + \bar{E}(\theta_B - 2)\theta_B}\Lambda \tag{30}$$

Due to the linearly varying strain assumption for the actuator in the bending case and the simpler, constant strain assumption for the extension case, these cases are not related through a simple numeric factor (e.g., α), as they were when the actuators were bonded on the surface.

The static elastic model for the six common cases of surface-bonded and embedded segmented piezoelectric actuators exciting extension and bending in the substructure have now been derived. The relevant results for the strains and forces are summarized in Table 1.

Table 1 Piezoelectric and substructure strains and applied forces for various actuator geometries

	Surface-bonded Extension ($\alpha=2$) Bending ($\alpha=6$)		Embedded Extension	Embedded Bending
	Perfect bond	Finite thickness bond	Perfect bond	Perfect bond
Strain in the piezoelectric $\epsilon_C =$	$\frac{\psi}{\psi+\alpha}[\bar{\epsilon}_+ + \bar{\epsilon}_- \tilde{x}] + \frac{\alpha}{\psi+\alpha}\Lambda$	$\frac{\psi}{\psi+\alpha}[\bar{\epsilon}_+ + \epsilon_- \tilde{x}] - \frac{\psi}{(\psi+\alpha)}\left[\bar{\epsilon}_+ \frac{\cosh\Gamma\tilde{x}}{\cosh\Gamma} + \bar{\epsilon}_- \frac{\sinh\Gamma\tilde{x}}{\sinh\Gamma}\right] + \left[\frac{\alpha}{\psi+\alpha} + \frac{\psi\cosh\Gamma\tilde{x}}{(\psi+\alpha)\cosh\Gamma}\right]\Lambda$	$\frac{\bar{E}(\theta_B-2)}{2+\bar{E}(\theta_B-2)}[\bar{\epsilon}_+ + \bar{\epsilon}_- \tilde{x}] + \frac{2}{2+\bar{E}(\theta_B-2)}\Lambda$	$\frac{2\psi\theta_B\bar{I}z/t_C}{24\theta_Z^2+\psi\theta_B^2\bar{I}+2}[\bar{\epsilon}_+ + \bar{\epsilon}_- \tilde{x}] + \frac{24\theta_Z z/t_C}{24\theta_Z^2+\psi\theta_B^2\bar{I}+2}\Lambda$
Strain in the substructure $\epsilon_B^s =$	$\frac{\psi}{\psi+\alpha}[\bar{\epsilon}_+ \bar{\epsilon}_- \tilde{x}] + \frac{\alpha}{\psi+\alpha}\Lambda$	$\frac{\psi}{\psi+\alpha}[\bar{\epsilon}_+ + \epsilon_- \tilde{x}] + \frac{\alpha}{(\psi+\alpha)}\left[\bar{\epsilon}_+ \frac{\cosh\Gamma\tilde{x}}{\cosh\Gamma} + \bar{\epsilon}_- \frac{\sinh\Gamma\tilde{x}}{\sinh\Gamma}\right] + \left[\frac{\alpha}{\psi+\alpha} + \frac{\alpha\cosh\Gamma\tilde{x}}{(\psi+\alpha)\cosh\Gamma}\right]\Lambda$	$\frac{\bar{E}(\theta_B-2)}{2+\bar{E}(\theta_B-2)}[\bar{\epsilon}_+ + \bar{\epsilon}_- \tilde{x}] + \frac{2}{2+\bar{E}(\theta_B-2)}\Lambda$	$\frac{2\psi\theta_B\bar{I}z/t_C}{24\theta_Z^2+\psi\theta_B^2\bar{I}+2}[\bar{\epsilon}_+ + \bar{\epsilon}_- \tilde{x}] + \frac{24\theta_Z z/t_C}{24\theta_Z^2+\psi\theta_B^2\bar{I}+2}\Lambda$
Applied force or moment	$F=\frac{E_B t_B b}{\psi+\alpha}[\bar{\epsilon}_+ + \bar{\epsilon}_- \tilde{x}] - \frac{E_B t_B b}{\psi+\alpha}\Lambda$	$\tau=\frac{G}{\bar{t}_S\Gamma}\left[\bar{\epsilon}_+ \frac{\sinh\Gamma\tilde{x}}{\cosh\Gamma} + \bar{\epsilon}_- \frac{\cosh\Gamma\tilde{x}}{\sinh\Gamma}\right] - \frac{G}{\bar{t}_S r}\frac{\sinh\Gamma\tilde{x}}{\cosh\Gamma}\Lambda$	$F=\frac{(\theta_B-2)E_B t_B b}{2\theta_B+\bar{E}(\theta_B-2)\theta_B} \times [\bar{\epsilon}_+ + \bar{\epsilon}_- \tilde{x}] - \frac{(\theta_B-2)E_B t_B b}{2\theta_B+\bar{E}(\theta_B-2)\theta_B}\Lambda$	$M_0=\frac{(12\theta_Z^2+1)\bar{I}E_B t_B^2 b}{3(24\theta_Z^2+\psi\theta_B^2\bar{I}+2)} \times [\bar{\epsilon}_+ + \bar{\epsilon}_- \tilde{x}] - \frac{2\theta_Z\theta_B\bar{I}E_B t_B^2 b}{24\theta_Z^2+\psi\theta_B^2\bar{I}+2}\Lambda$
Notes	$\Gamma^2=\frac{\bar{G}\theta_S}{\bar{t}_S^2}\left[\frac{\psi+\alpha}{\psi}\right]$	$\bar{\epsilon}_+ = \frac{\epsilon_B^{s+} + \epsilon_B^{s-}}{2}$	$\bar{\epsilon}_- = \frac{\epsilon_B^{s+} - \epsilon_B^{s-}}{2}$	

Dynamic Models of Piezoelectric/Substructure Coupling

The detailed models of the piezoelectric coupled to a substructure can now be integrated into a larger dynamic model of the system. In principle, a coupled dynamic model of the substructure and actuator should be developed. However, under the assumptions that the actuator mass is small relative to the total mass of the system and that any resonances of the actuator are higher than the frequencies of interest, the actuator will act quasistatically compared to the structure. In this case, the mechanical dynamics of the actuator can be ignored and the static models derived previously can be used to examine the influence of the actuator on the dynamics of the substructure. Two steps are necessary: 1) a dynamic model of the structure is developed using any conventional technique, and 2) the influence of the actuators is incorporated by calculating either the applied strain [Eqs. (13), (18), (27), or (29)] or generalized applied force [Eqs. (15), (19), (28), or (30)] on the substructure. Since dynamic models more readily incorporate the applied forces, this is the preferable approach in most cases.

In this section, a coupled dynamic model will be developed for a substructure in bending with both surface-bonded and embedded actuators. In this example, a cantilevered beam will be modeled using a single mode Rayleigh-Ritz model.[12]

Dynamic Response due to Surface-Bonded Actuators

In the case of an actuator bonded to the surface of the beam by a layer of finite stiffness, the generalized applied force is a surface shear. Figure 4 shows a cantilevered beam being acted upon by such a surface shear created by a pair of actuators in such a way as to excite bending. The forcing of the piezoelectric actuator appears in the Rayleigh-Ritz equation of motion for the beam[12] through the modal force Q,

$$Q=\int_{(\bar{a}-\bar{m})}^{(\bar{a}+\bar{m})} \tau b t_B \tilde{\varphi}'\, d\tilde{x} \tag{31}$$

where the only unknown is τ, the shear stress applied by the piezoelectrics that can be found from Eq. (15). Before substituting for τ, the boundary conditions ϵ_B^{s+} and ϵ_B^{s-} (i.e., the strain present in the beam in the absence of the piezoelectric) must be evaluated. In this case, these strains are due to the modal motion and can be expressed in terms of the

generalized coordinate q as

$$\epsilon_B^s = -\frac{t_B}{2}\frac{\partial^2 w}{\partial x^2} = -\frac{t_B}{2}\frac{\partial^2 \varphi}{\partial x^2}\, q \tag{32}$$

Using Eq. (32) to substitute for ϵ_B^{s+} and ϵ_B^{s-} in Eq. (15), inserting the resulting expression for τ in Eq. (31), and integrating yield

$$Q = \frac{-Gbt_B^2}{4\bar{t}_S\Gamma\ell^2}\left[\frac{\varphi''(\tilde{a}+\tilde{m})-\varphi''(\tilde{a}-\tilde{m})}{\sinh\Gamma} I_C + \frac{\varphi''(\tilde{a}+\tilde{m})+\varphi''(\tilde{a}-\tilde{m})}{\cosh\Gamma} I_S\right] q - \frac{Gbt_B}{\bar{t}_S\Gamma}\cdot\left(\frac{I_S}{\cosh\Gamma}\right)\Lambda \tag{33a}$$

$$= K_{\text{PIEZO}}\, q + Q_V \Lambda \tag{33b}$$

where

$$I_C = \int_{(\tilde{a}-\tilde{m})}^{(\tilde{a}+\tilde{m})} \cosh\left[\frac{2\Gamma}{\bar{L}}(\tilde{x}-\tilde{a})\right]\varphi'(\tilde{x})\,d\tilde{x} \tag{34}$$

$$I_S = \int_{(\tilde{a}-\tilde{m})}^{(\tilde{a}+\tilde{m})} \sinh\left[\frac{2\Gamma}{\bar{L}}(\tilde{x}-\tilde{a})\right]\varphi'(\tilde{x})\,d\tilde{x} \tag{35}$$

Equation (33) expresses the modal force applied by the piezoelectric in terms of both the motion of the beam and the applied voltage. The first term is proportional to q and expresses the added passive modal stiffness, K_{PIEZO}, due to bonding the piezoelectrics to the beam. The second term is the effective forcing term and depends on the piezoelectric strain term Λ, which is proportional to the applied voltage V.

The resulting equation of motion for the single-mode model of the piezoelectric-beam system is

$$M\ddot{q} + B\dot{q} + (K + K_{\text{PIEZO}})q = Q_V\Lambda = Q_V\frac{d_{31}V}{t_C} \tag{36}$$

which can be used to predict the response of a beam.

Dynamic Response due to Embedded Actuators

A similar procedure will now be used to calculate the response induced by a pair of actuators embedded within a cantilevered beam. In this case, however, the expression for the Rayleigh-Ritz modal force depends on M_0, the moment applied to the beam at the left and right ends of the piezoelectric, and the slope of the beam at those two points,

$$Q = \left[\left(\frac{M_0}{\ell}\tilde{\varphi}'\right)\Big|_+ - \left(\frac{M_0}{\ell}\tilde{\varphi}'\right)\Big|_-\right] \tag{37}$$

Equation (23), which expresses the moment in terms of the applied force (ΔF and $\bar{F}$), is substituted in Eq. (37). It should be noted that in deriving Eq. (37), the concentrated applied moment M_0, and not a distributed moment, is used since, for perfectly bonded actuators, the generalized force is applied only at the ends of the actuator and not along its entire length.

If we substitute Eqs. (24) and (25) for ΔF and $\bar{F}$ and once again use Eq. (32) to express the boundary values for the strain ϵ_B^{s+} and ϵ_B^{s-} in terms of the modal displacement q, the modal force Q is

$$Q = \frac{-E_B t_B^3 b\bar{I}(12\theta_Z^2+1)}{6\ell^3(24\theta_Z^2+\psi\theta_B^2\bar{I}+2)}\left[\varphi''(\tilde{a}+\tilde{m})\cdot\varphi'(\tilde{a}+\tilde{m}) - \varphi''(\tilde{a}-\tilde{m})\cdot\varphi'(\tilde{a}-\tilde{m})\right] q - \frac{2E_B t_B^2 b\theta_Z\theta_B\bar{I}}{\ell(24\theta_Z^2+\psi\theta_B^2\bar{I}+2)} \times\left[\varphi'(\tilde{a}+\tilde{m})-\varphi'(\tilde{a}-\tilde{m})\right]\Lambda \tag{38a}$$

$$= -K_{\text{PIEZO}}\, q + Q_V\Lambda \tag{38b}$$

The similarities between Eqs. (33) and (38) are readily apparent. The modal force consists of an added passive stiffness term and a forcing term proportional to the voltage applied across the actuators. Since material is removed from the beam in order to insert the actuators, the total stiffness $K + K_{\text{PIEZO}}$ might be greater or less than the stiffness of a beam without the embedded actuators, depending on the relative stiffness of the piezoelectrics and the substructural material.

Note that the second term of Eq. (38) is proportional to the difference between the slope of the beam at the two ends of the actuator. Therefore, in order to maximize the modal force applied to the beam, it is desirable to place the actuators in regions of high average strain. This design guidance, that piezoelectric actuators which strain the substructure should optimally be placed in regions of high average strain, is analogous to the more familiar observations that linear force actuators should optimally be placed in regions of large displacement and that torque actuators should be placed in regions with large modal slope.

Dynamic Response due to Perfectly Bonded Surface Actuators

In cases where surface-bonded actuators are bonded to a beam through a thin shear layer such that $\Gamma > 30$, the perfectly bonded static model can be used. As in the case of the embedded actuator, the modal force is again dependent on the concentrated moment applied at the ends of the piezoelectric [Eq. (20)]. The substitution of Eq. (20) into Eq. (37), and the substitution of Eq. (19) gives the expression for the modal force Q,

$$Q = -\frac{E_B t_B^3 b}{2\ell^3(6+\psi)}\left[\tilde{\varphi}''(\tilde{a}+\tilde{m})\cdot\tilde{\varphi}'(\tilde{a}+\tilde{m}) - \tilde{\varphi}''(\tilde{a}-\tilde{m})\cdot\tilde{\varphi}'(\tilde{a}-\tilde{m})\right] q - \frac{E_B t_B^2 b}{\ell(6+\psi)} \times\left[\tilde{\varphi}'(\tilde{a}+\tilde{m})-\tilde{\varphi}'(\tilde{a}-\tilde{m})\right]\Lambda \tag{39a}$$

$$= -K_{\text{PIEZO}}\, q + Q_V\Lambda \tag{39b}$$

Examples of incorporating the three types of piezoelectric substructure coupling models have now been presented. The models for excitation of extension in the substructure can be developed in an analogous manner. These models can be used to estimate the effects of the piezoelectric on the structural modes of interest and will be used below to examine scaling, actuator choice and placement, and to correlate with experimental data.

Scaling Analysis

Having derived the static and dynamic piezoelectric substructure coupling models, a reasonable question remains as to the effectiveness of piezoelectrics in influencing the dynamics of structures of realistic size. This question centers on the capability of the authority of the actuator to scale as the size of the structure is increased. To address this ques-

tion, a scaling analysis is performed on a typical model structure, a rectangular cross-section cantilevered beam, excited by a single piezoelectric actuator. For the purposes of this analysis, the perfectly bonded surface actuator model [Eq. (39)] will be used and attention will be focused on the forcing term $Q_V\Lambda$.

The modal damping ζ is a nondimensional measure of the dynamics of a system that can be interpreted as the fraction of the stiffness force acting to damp the system. If the modal damping is due to rate feedback to an actuator, then the achieved ζ is a nondimensional measure of the effectiveness of that actuator. In rate feedback to a piezoelectric, the applied voltage is equal to the beam velocity times a gain λ_V

$$V=\lambda_V\dot{q} \tag{40}$$

and therefore the applied piezoelectric strain is

$$\Lambda=\frac{d_{31}V}{t_C}=\frac{d_{31}\lambda_V}{t_C}\,\dot{q} \tag{41}$$

The modal force $Q_V\Lambda$ is now proportional to the velocity of the beam. In order to determine the achieved ζ, the modal force [Eq. (39)] is equated to the damping force

$$2\zeta M\omega_0\dot{q}=Q_V\Lambda \tag{42}$$

and the damping ζ that is obtained from the rate feedback to the piezoelectric actuator is equal to

$$\zeta=\frac{d_{31}\lambda_V}{2M\omega_0 t_C\ell}\cdot\frac{E_B t_B^2 b}{6+\psi}\cdot[\tilde{\varphi}'(\tilde{a}+\tilde{m})-\tilde{\varphi}'(\tilde{a}-\tilde{m})] \tag{43}$$

It is clear that if the gain λ_V is increased, so is the damping. Therefore, in order to determine a maximum value of ζ, it is necessary to impose a maximum value of λ_V, which is set by the actuator saturation limits. In this case, the appropriate upper limit is the field necessary to depole or destroy the piezoelectric properties of the actuator. The maximum field $\mathcal{E}_{\mathrm{MAX}}$ that can be applied is related to the gain as

$$\lambda_{V_{\mathrm{MAX}}}=\frac{V_{\mathrm{MAX}}}{\dot{q}_{\mathrm{MAX}}}=\frac{\mathcal{E}_{\mathrm{MAX}}t_C}{\dot{q}_{\mathrm{MAX}}}=\frac{\mathcal{E}_{\mathrm{MAX}}t_C}{\omega_0 q_{\mathrm{MAX}}} \tag{44}$$

where the assumption has been made that motion of interest is at the resonance frequency. Substituting Eq. (44) into Eq. (43) and using the expression for the modal stiffness of a rectangular cross-section beam results in

$$K=\frac{E_B I_B}{\ell^3}\int_0^1(\tilde{\varphi}'')^2\mathrm{d}\tilde{x}=\frac{E_B b t_B^3}{12\ell^3}\,\bar{K}=M\omega_0^2 \tag{45}$$

The final expression for the achieved modal damping at actuator saturation is

$$\zeta=\frac{t_B}{q_{\mathrm{MAX}}}\left(\frac{\ell}{t_B}\right)^2\left[\frac{\tilde{\varphi}'(\tilde{a}+\tilde{m})-\tilde{\varphi}'(\tilde{a}-\tilde{m})}{\bar{K}}\right]\times(\mathcal{E}_{\mathrm{MAX}}d_{31})\left(\frac{6}{6+(E_B t_B/E_C t_C)}\right) \tag{46}$$

The first term in Eq. (46) is the inverse of the normalized tip amplitude. The second term is the slenderness ratio of the beam, squared. These two geometric terms remain constant as the dimensions of the system are scaled. The third term contains factors involving the nondimensional mode shape and stays constant if the ratio of the lengths of the piezoelectric actuator to the beam remains constant. This can be done either by increasing the length of the piezoelectric or by using more piezoelectrics whose total length is a fixed fraction of the structural length. This term also gives guidance as to where to place the piezoelectric actuator optimally along the beam; i.e., they should span regions of high average strain. The fourth term is just the maximum piezoelectric strain that can be obtained from the actuators and is a material property independent of scale. The fifth term depends on the stiffness ratio of the beam and the piezoelectric and stays constant if the thickness of the piezoelectric is increased as the beam is scaled. Equation (46) indicates that, as the system is scaled in three dimensions, the damping obtained through rate feedback to the piezoelectric actuators remains constant if the ratio of actuator dimensions to beam dimensions remains constant. Thus, the effectiveness of piezoelectric actuators is independent of the scale of the substructure.

Design and Manufacture

In order to establish the feasibility of integrating distributed segmented piezoelectric actuators into a structure and to provide specimens for experimental verification of the analytic models presented above, three dynamic test specimens were manufactured. These consisted of an aluminum beam with two surface-mounted piezoelectric actuators (PZA), a glass/epoxy beam with two embedded PZA's and a graphite/epoxy beam with a single embedded PZA. Here, a PZA is defined to consist of two piezoelectrics, bonded or embedded at opposite but equal distance from the neutral axis of a beam and driven 180 deg out of phase. The net effect of a PZA is to impart a localized moment to the beam. In addition, glass/epoxy static test coupons with a single embedded PZA were also manufactured for static stiffness and strength testing. The four different types of specimens are shown in Fig. 5, and their dimensions and properties are listed in Table 2. Before going into the details of the manufacture of each specimen, certain issues common to the design of all the test specimens, including the choice of the actuator locations and the selection of the piezoelectric material used, will be discussed.

Location of Actuators

The choice of actuator location is an important issue in the design of actively controlled structures. The actuators should be placed at the locations to excite the desired modes most effectively. For the test specimens previously described, these are the first and second cantilevered bending modes. As was shown in Eqs. (38) and (46), piezoelectric actuators, which locally strain the substructure, should be placed in regions of high average strain and away from areas of zero strain. The location of these "strain nodes" are determined by twice differentiating the analytic expressions for the beam cantilever modes and finding the zero-crossing points of the

Table 2 Properties and dimensions of test specimens

	Dynamic			Static
	Aluminum	Glass	Graphite	Glass
Length ℓ, m	0.4	0.28	0.35	0.32
Width b, mm	38	38	50	50
Thickness t_B, mm	3.18	2.54	2.95	2.54
Flexural modulus E_B, GPa	70	29.6	71.6	27.8
First PZA location, mm	5-43	10-48	10-48	141-179
Second PZA location, mm	101-140	77-115	n/a	n/a

Table 3 Properties of various piezoelectric materials

	PZT G-1195	PZT HST-41	PZT G-1278	PVDF
Curie temperature, °C	360	270	190	100
$\mathcal{E}_{MAX}$, V/m	600×10^{3}	600×10^{3}	600×10^{3}	40×10^{6}
d_{31}, m/V	190×10^{-12}	157×10^{-12}	250×10^{-12}	23×10^{-12}
E_C, N/m^2	63×10^{9}	70×10^{9}	60×10^{9}	3×10^{9}
Effectiveness	40×10^{-6}	34×10^{-6}	50×10^{-6}	21×10^{-6}
Effectiveness/field, m/V	67×10^{-12}	56×10^{-12}	83×10^{-12}	553×10^{-15}

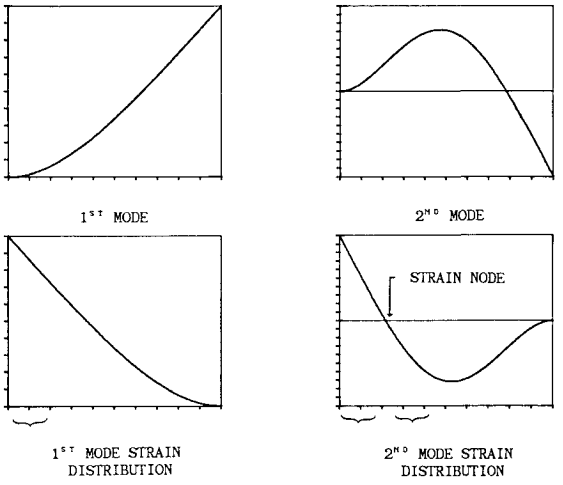

Fig. 6 Mode shapes and surface strain distributions for first and second cantilevered beam modes.

resulting functions. As can be seen in Fig. 6, the first mode has no strain nodes. Therefore, if this were the only mode to be excited, the actuators could be placed anywhere along the beam. For maximum effectiveness, they would be placed as near to the root as possible. The second mode has a strain node at $x=0.216\ell$. The PZA's must be placed away from this point, so that the strain applied over the entire length of the actuator has a constant phase with respect to the homogeneous strain in the beam in this mode. If not, the modal force produced by the actuator will be decreased, since one section of the actuator will be opposing the other. The exact choice of location for the actuators for each specimen will be described in the following sections.

This reasoning also indicates why it is necessary to use segmented actuators for the control of flexible structures. For the second mode of a cantilevered beam, a PZA located at $x<0.216\ell$ must be driven 180 deg out of phase with a PZA located at $x>0.216\ell$. All flexible structures will have such strain nodes in all their elastic modes above the first. Therefore, in order to control the flexural modes effectively, it is necessary to control independently the driving voltage applied to each PZA. This cannot be done if the actuator is continuous over the length of the beam.

Selection of Actuator Material

Having determined the appropriate criteria for placing the actuators, we will discuss the choice of the piezoelectric material. A wide variety of piezoelectric materials are currently available, including piezoelectric film, piezoceramics, and piezoelectric bimorph elements. In the selection of the one to be used in the manufacture of the dynamic test specimens, certain criteria had to be considered. From a manufacturing viewpoint, a surface-bonded actuator can be made from any type of piezoelectric material that can contour to the surface. It is, of course, desirable to use a piezoelectric material which has a high piezoelectric-mechanical coupling effectiveness. This effectiveness parameter is defined as being equal to the last two terms in Eq. (46),

$$\text{Effectiveness} = (\mathcal{E}_{MAX} d_{31})\left[\frac{\alpha}{\alpha + (E_B t_B / E_C t_C)}\right] \quad (47)$$

This nondimensional parameter is simply the maximum amount of strain that an actuator can transmit to the substructure under ideally bonded, static conditions, when the maximum allowable field $\mathcal{E}_{MAX}$ is applied across the piezoelectric. It is the product of the maximum strain that can be created in the piezoelectric, which depends on the piezoelectric properties of the actuator, and a quotient that expresses how much of this strain can be imparted to the substructure, which depends on the mechanical properties of the actuator and substructure. A high $\mathcal{E}_{MAX}$ is clearly a desirable feature, so that a large field can be applied to the piezoelectric before depoling occurs, which destroys the piezoelectric properties of the material. An actuator with a high effectiveness must also have a high piezoelectric constant d_{31}, since for a large d_{31} a large strain is produced for a small voltage. If d_{31} is small, then a large voltage will be required to produce strain in the piezoelectric. In addition, the piezoelectric must also have a high modulus of elasticity E_C. If E_C is small compared to the modulus of the substructure, then only a small fraction of the strain produced in the piezoelectric will be transferred to the substructure. Table 3 shows the effectiveness of various piezoelectric materials, assuming that bending ($\alpha=6$) is excited in an aluminum substructure whose thickness is 10 times the piezoelectric thickness. If voltage that can be applied across the piezoelectric is limited, then the effectiveness per field should also be considered in the selection of the piezoelectric material, since this parameter allows comparison of the effectiveness of various piezoelectric materials when an equal electric field is applied. The value of this parameter is also given in Table 3.

The design of the laminated composite test specimens requires that the choice of actuator material satisfies two additional criteria: 1) the piezoelectric material must have an elastic modulus comparable to the modulus of a typical advanced composite laminate so as not to create an effective discontinuity or void in the laminate and 2) the Curie temperature (the temperature above which the piezoelectric permanently loses its piezoelectric properties) of the actuator material must be higher than the curing temperature of the composite. If this is not the case, the piezoelectric nature of the material will be destroyed during the laminate curing process.

The three criteria listed (effectiveness, elastic modulus, and Curie temperature) eliminated piezoelectric film as a candidate for the actuator material, since it has a low effectiveness/field, a low elastic modulus, and a low Curie temperature. The choice was then reduced to various varieties of piezoelectric ceramics of which G-1195, manufactured by Piezo Electric Products, was selected. The ceramics actually used as actuators had dimensions of $38.1\times15.2\times0.25$ mm. Since the thickness of this actuator is also the nominal thickness of one glass/epoxy ply or two graphite/epoxy plies, this will simplify the manufacturing of the composite test specimens.

Manufacture of the Aluminum Test Specimen

The dimensions and elastic properties of the aluminum test specimen are given in Table 2. Eight piezoceramics, forming four PZA's, were bonded to the beam. Each pair of PZA's was bonded side by side to form two sets of actuators (Fig. 5). As can be seen from the table, the actuators were located away from the second-mode strain node.

This test specimen presented three manufacturing difficulties: 1) electrical contact had to be made with both sides of the piezoelectrics after these were bonded to the beam; 2) the piezoelectrics had to be electrically isolated from the beam in order to allow a voltage to be applied across the actuator; and 3) the uniformity of the bonding layer thickness between the piezoelectrics and the beam had to be maintained, since the theoretical model required this dimension to be a known constant.

The first two points are important because, as explained earlier, segmented piezoelectric actuators require the voltage to be applied across the thickness of each piezoelectric independently of the others. This was accomplished by using a nonconductive epoxy and drilling small holes in the substructure underneath each actuator through which the leads were threaded. In order to avoid any possibility of a short circuit through the beam, the entire beam was anodized.

The piezoelectrics were bonded to the beam using EPY-150, a 24 h room temperature curing epoxy manufactured by BLH Electronics. Emerson & Cuming IG-101 microballoons of a maximum diameter of 175 μm were mixed into the epoxy. In this way, when pressure was applied during the cure, the thickness of the bonding layer was reduced to the diameter of the microballons, thus insuring a constant bonding layer thickness.

Manufacture of the Glass/Epoxy Test Specimens

The dynamic glass/epoxy test specimen was manufactured using 3M 1002 prepreg material. The dimensions and properties of this test specimen are given in Table 2, along with the actuator locations. Four G-1195 piezoceramics, forming two PZA's, were embedded inside the beam. Once again, the actuators are located away from the second mode strain node.

A $[0/90/0/90/0]_S$ laminate was used. Each ply of this laminate had a nominal thickness of 0.254 mm. This is equal to both the nominal thickness of the piezoceramic and the thickness of the attached leads. Therefore, by cutting holes of the exact dimensions of the piezoceramics and the leads, they could be inserted inside the laminate without causing any change in the nominal thickness. The piezoceramics were embedded in the third and eighth plies. Slits for the leads bonded to the piezoelectric were cut in the 90 deg plies above and below each embedded piezoceramic, i.e., in the second, fourth, eighth, and tenth plies. The leads led out to the side of the specimen, normal to the axis of strain. The piezoelectric-lead assemblies were set in the prepreg during layup. The standard curing procedure recommended by the manufacturer was used. Teflon was wrapped around the leads outside the laminate in order to prevent any excess epoxy that might flow during the curing process from bonding to the leads.

In addition to the dynamic glass/epoxy test specimen, four static test specimens were constructed in order to determine how the presence of the embedded actuator affected the strength and stiffness of the laminate. The dimensions of these specimens are given in Table 2. Two were constructed in the same manner as the dynamic specimens, except that only one PZA, located in the center of the specimen, was embedded. The other two had no embedded PZA and were used as controls. Strain gages were attached in the region of the PZA and in the far field in order to measure the material modulus and the effect of the piezoelectric on the local strain distribution.

Manufacture of the Graphite/Epoxy Test Specimen

The manufacture of the graphite/epoxy test specimen was very similar to the manufacture of the glass/epoxy specimens. Only one PZA was embedded, since the purpose of this test specimen was primarily to verify the procedure developed to insulate the piezoelectric layer on the load transfer from the piezoelectric to the beam. The specimen consisted of a $[0_2/90_7/0_2]_S$ laminate manufactured using Hercules AS4/3501-6 graphite/epoxy prepreg. The dimensions and properties are given in Table 2.

As was mentioned earlier, the problem with embedding piezoelectrics inside a graphite/epoxy beam is that the graphite fibers electrically short-circuit the piezoelectric by making contact with the electrodes or the bonded leads. To prevent this, 0.125 mm thick Kapton insulated leads manufactured by Micromat were soldered to the actuator and the entire piezoelectric-lead assembly was wrapped in Kapton film manufactured by DuPont. The isulated piezoelectric was then embedded inside the laminate. The film was bonded to the piezoelectric using acrylic expoxy that cured during the regular cure cycle of the graphite/epoxy. Since the piezoelectric thickness (0.25 mm) is twice the thickness of a nominal ply of graphite/epoxy and the insulating film is 0.05 mm thick, three plies were cut in order to make room for each insulated piezoelectric. The ceramics were embedded between the 4th and 8th and between the 15th and 19th plies. Slits for the leads leading out to the side of the specimen were cut in the plies directly above and below the piezoelectrics. Finally, the laminate was cured using the manufacturer-recommended cure cycle.

Experimental Procedure and Dynamic Test Results

The dynamic testing procedure for all test specimens will be described and the experimental data presented. In order to test for the effective coupling of the ceramics to the beam, specimens were excited sinusoidally at resonance. The response to this excitation was then compared to the predicted response for the specimens. When driven at resonance, the second-order system represented by Eq. (36) responds with amplitude

$$\text{Amplitude} = \frac{Q_V V}{2(K + K_{\text{PIEZO}})\zeta} \tag{48}$$

where ζ is the modal damping of the structure. For the purposes of analytically predicting the amplitude of response, the beam stiffness K can be easily calculated using the assumed mode shape and Q_V and K_{PIEZO} can be determined from Eq. (37) or Eq. (42). The passive beam structural damping ζ is difficult to predict. In order to minimize the uncertainty in the experiment, ζ was determined by independent experiments. With the damping determined, all the terms in Eq. (48) are known and the response of the test specimens at resonance can be determined as a function of the applied voltage. This is then compared to the experimentally measured amplitude obtained by performing sinusoidal excitation tests on the test specimens for a fixed excitation voltage.

All tests were performed with the specimens vertically clamped to a steel base, which was effective in providing a cantilevered boundary condition in that the difference between the actual and the theoretical first mode frequency was less than 2%. In the forced response tests, the PZA's in the specimen were excited sinusoidally by an amplifier configured for a high impedance load. The response of the test specimen was measured using an Endevco 2222C accelerometer bonded to the tip of the beam. The accelerometer signal was divided by the frequency squared to obtain the tip amplitude. The damping in each specimen was experimentally determined by performing an independent series of transient ringdown tests for each specimen at both first and sec-

ond bending frequencies. These transient response data were digitized and fitted in the time domain using a least squares algorithm to determine the modal damping.

The test data from the various forced response experiments will be presented in two forms: 1) figures showing the theoretical and typical experimental response for each specimen will be presented and 2) an explicit comparison of the theoretical and experimental results will be made by comparing the coefficient Q_V, the constant that relates voltage and modal force [Eq. (33)]. This term should be constant for each specimen. The analytic prediction for Q_V can be found using either Eq. (33) or (38) as appropriate. The experimental value can be determined by solving Eq. (48),

$$Q_V = \text{Amplitude} \cdot \frac{2\zeta(K + K_{\text{PIEZO}})}{V} \tag{49}$$

and inserting the experimentally measured amplitude, damping, and voltage and the Rayleigh-Ritz predicted stiffness value.

Aluminum Beam

The aluminum beam was excited in its first and second mode using each actuator set individually and then both sets simultaneously. For this last case, the voltages applied to both actuator sets were always equal in magnitude. The driving voltages were equal in phase for the first-mode tests and were set 180 deg out of phase for the second-mode tests to account for the presence of the strain node between the actuator locations.

Figure 7 shows the results of the sine dwell tests for the first-mode test using all the piezoelectric actuators. The actual measured tip amplitude of the beam, as well as the predicted amplitude based on the analysis described above [Eq. (33)], is shown. As was mentioned earlier, the actual measured damping varied with amplitude. For this specimen, the damping ratio was found to increase approximately linearly with amplitude from $\zeta = 0.0035$ at 0 normalized amplitude to $\zeta = 0.0079$ at 3.22 normalized amplitude. This accounts for the nonproportionality of the predicted response to the applied voltage at high amplitudes. As can be seen from Fig. 7, there is very good agreement with the actual test results. These results are typical of all the tests performed using the various actuator combinations.

Table 4 shows the analytic and average experimental values of Q_V for the six tests performed on the aluminum specimen. It is seen from this table that the PZA's closer to the root excited a greater response since they are located in a region of higher strain than the other PZA's for both the first and second modes. Also, when all PZA's are excited with equal amplitude, their responses add linearly. This is not surprising since the analytic model is linear and, therefore, the principal of superposition of actuator effectiveness is valid.

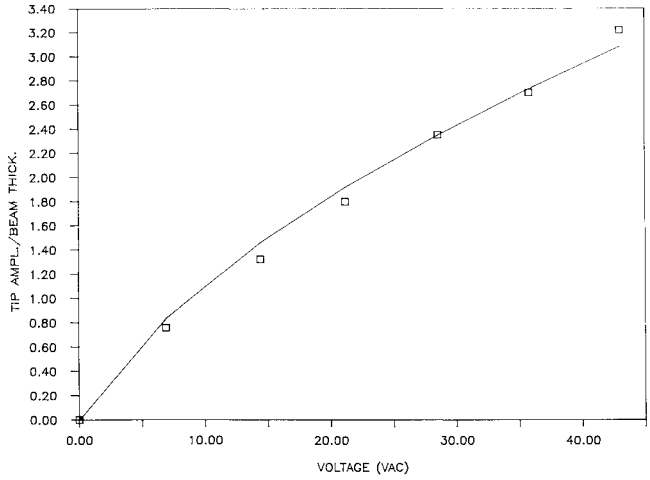

Fig. 7 Response of first bending mode of aluminum beam using all PZA's.

Glass/Epoxy Beam

An identical series of sine dwell tests to those perfomed on the aluminum beam were performed on the glass/epoxy specimen. Figure 8 shows the results of the sine dwell test for the first mode when excited by both PZA's, along with the analytically predicted response. The damping ratio ζ for this specimen was found to be approximately constant with amplitude and was equal to 0.006. The predicted response is in good agreement with the experimental results. This is not surprising even though a very simple compatible strain model was used in the prediction of the response, since the small interlaminar bonding layer reduces the shear lag in the system to negligible levels.

Graphite/Epoxy Beam

The perfectly bonded model [Eq. (38)] was again used to predict the behavior of the graphite/epoxy beam when excited by the embedded piezoelectric actuator. The primary purpose of this series of sine dwell tests was to verify that the presence of the Kapton film around the piezoelectric did not reduce its effectiveness as an actuator, since the Kapton could act as a shear layer between the actuator and the composite. Figure 9 shows the results of the first-mode sine dwell test performed on the graphite/epoxy beam, along with the

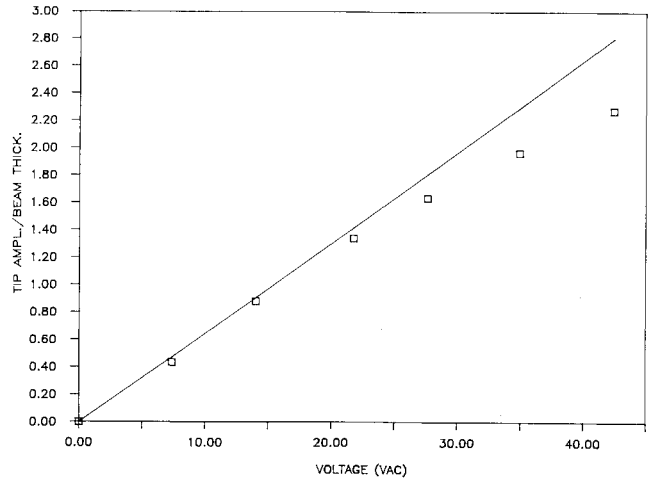

Fig. 8 Response of first bending mode of glass/epoxy beam using all PZA's.

Table 4 Theoretical and experimental Q_V

Specimen	Mode	PMA	Theory	Experimental average	Δ, %
Aluminum	1	1	1.78	1.81	−1.7
		2	1.09	1.21	−9.9
		1 and 2	2.91	3.02	−3.6
	2	1	4.43	4.45	−0.5
		2	2.15	1.99	8.0
		1 and 2	6.34	6.44	−1.6
Glass	1	1	0.68	0.75	−9.3
		2	0.42	0.47	−5.0
		1 and 2	1.10	1.22	−9.8
	2	1	1.22	1.32	−7.6
		2	1.13	1.21	−6.6
		1 and 2	2.03	2.53	−19.7
Graphite	1		0.54	0.55	−1.0

predicted response. As with the glass/epoxy beam, the damping ratio ζ was constant with amplitude and equal to 0.005. Table 4 shows the analytic and experimental value of Q_V. As can be seen from the figure, the experimental results are in excellent agreement with the analytic model. Therefore, the presence of the Kapton insulation does not reduce the effectiveness of the actuator.

Static Testing Procedure and Results

When the piezoelectrics were embedded inside the glass/epoxy laminate, their presence caused a discontinuity in the fibers of the ply in which they were embedded. In order to obtain a quantitative measure of the effect of the embedded actuator on the laminate properties, a series of static tests were conducted.

Table 5 Static elastic modulus and failure stresses

Specimen	Actuator	Modulus, GPa at gage 1	2	3	4	Failure stress, MPa
Control	None	31	34	32	32	615
Control	None	27	29	28	28	634
Embedded PZA	PMA	33	39	36	35	505
Embedded PZA	PMA	32	36	33	32	522
Predicted value			27.8			637

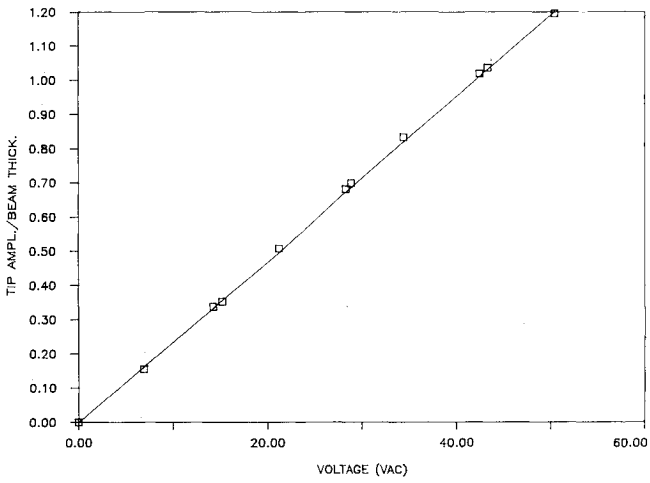

Fig. 9 Response of first bending mode of graphite/epoxy beam.

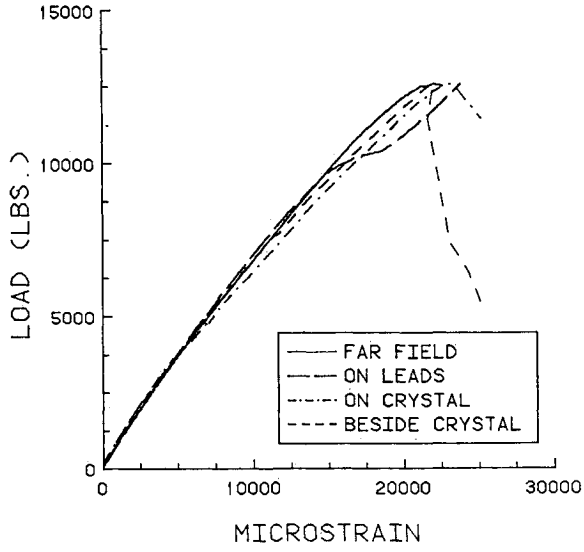

Fig. 10 Load vs strain for static glass/epoxy specimen with embedded actuator.

As described earlier, four static test specimens were manufactured. Strain gages were applied in the far field away from the actuator, as well as directly over the PZA, near its edges, and over the leads. Additionally, the distribution of the strain around the actuator was determined by using a photoelastic coating on some of the specimens. The testing procedure consisted of mounting the specimens on an Material Testing Systems (MTS) testing machine and applying a monotonic loading under stoke control at a rate of 0.04 in./min, until failure in, the specimen was detected.

Figure 10 shows typical load vs strain data for a specimen with an embedded PZA. Initial values for the global elastic modulus of all the specimens based on the strain data from each gage were obtained and are shown in Table 5. The theoretical value for the elastic modulus obtained from classical laminated plate theory is 27.8 GPa. Therefore, the presence of the ceramic does not have an effect on the elastic modulus of the laminate due to the high modulus of the piezoelectric (63 GPa), which allows the stress due to the applied load to be transferred to the piezoelectric through the epoxy matrix.

Table 5 also shows the value of the stress at which the laminates failed catastrophically. The predicted value is equal to 637 MPa and was obtained using a stress interaction criteria[13] assuming the laminate could still carry load after the first ply failure. This value agrees very well with the failure stresses of the unflawed laminates. However, the flawed laminates failed at a stress 20% less than the predicted value. This decrease in strength is large enough to require that it be taken into account in designing structures with embedded actuators.

Conclusions

Segmented piezoelectric actuators have been shown both analytically and experimentally to be a viable concept for dynamic vibration and shape control of structures. Because of their small size and high modulus, piezoelectrics bonded to or embedded in a structural member can be joined together in a highly distributed actuator network with a minimal effect on the passive structural properties of the member.

Static analyses for various actuator geometries were presented, leading to complete analytic solutions of the governing equations for each case. For the surface-bonded cases, both perfectly bonded and finite bonding layer models were presented and compared. For the embedded models, only the perfectly bonded case was presented, since the shear lag present in the thin interlaminar bonding layer is negligible.

The flexural static models for both surface-bonded and embedded actuators were integrated into dynamic models for a cantilevered Bernoulli-Euler beam. The forcing applied by the actuators was shown to consist of a passive stiffness component due to the presence of the actuator and a voltage-dependent component that relates to the ability of the piezoelectric actuator to impart a force on the structure. This coupling of the static and dynamic model led to the ability to predict the behavior of the beam under excitation from the piezoelectric actuators.

A scaling analysis was conducted for surface-bonded piezoelectrics exciting bending in a cantilevered beam. This analysis indicated that the nondimensional effectiveness of the piezoelectric actuator remains constant if the dimension of the piezoelectrics increase in scale with those of the structure. The scaling analysis also provides a systematic method based on maximizing the piezoelectric-mechanical effectiveness of the actuator and the substructure that can be used to select the piezoelectric actuator material.

A technique for selecting the location of a surface-bonded or embedded piezoelectric actuator based on the characteristics of the strain distribution of a structure was developed. This technique indicates that segmented actuators are always more effective than a continuous actuator since the output of each actuator can be individually controlled.

Manufacturing techniques for bonding or embedding segmented piezoelectric actuators were developed. These techniques allowed independent electrical contact to be made with each actuator and thus allowed the modal force due to each actuator to be independently controlled. Actuators were successfully embedded inside both glass/epoxy and graphite/epoxy laminates. For this latter case, the piezoelectrics were insulated from the graphite fibers by coating them with a Kapton film.

Finally, static tests to determine how the elastic properties of the composite are affected by the presence of an embedded actuator were carried out on glass/epoxy laminates. The results of these tests show that, although the modulus of the composite laminate is not affected by the actuator presence, the ultimate strength is reduced by approximately 20%.

In conclusion, all the tools necessary to use segmented piezoelectric actuators in embedded or surface-bonded geometries in bar and beamlike structures and the ability to predict, a priori, the performance of these actuators has been developed and can now be used for predicting the behavior of flexible structures with distributed piezoelectric actuators.

Acknowledgments

This research was supported by NASA Grant NAGW-21, with Mr. Samuel Venneri serving as Technical Monitor. The authors wish to thank Messrs. David Stampleman and Ron Spangler for their contribution in the manufacturing and testing phase of this research.

References

[1]Balas, M., "Active Control of Flexible Structures," *Journal of Optimization Theory and Applications*, Vol. 25, July 1978, pp. 415–436.

[2]Gibson, J. S., "The Riccati Integral Equations for Optimal Control Problems on Hilbert Spaces," *SIAM Journal on Control and Optimization*, Vol. 17, No. 4, July 1979, pp. 537–565.

[3]Ward, B. A. and Crawley, E. F., "A Hierarchical Control Architecture for Large Flexible Structures," Space Systems Laboratory, Massachusetts Institute of Technology, Cambridge, MA, Rept. MIT-SSL 18-85, Aug. 1985.

[4]von Flotow, A. H., "Low-Authority Control Synthesis for Large Space Structures Using Disturbance Propagation Concepts," AIAA Paper 85-0630, April 1985.

[5]Fabunni, J. A., "Forced Vibration of a Single Stage Axial Compressor Rotor," *Journal of Engineering for Power*, Vol. 102, No. 2, April 1980, pp. 322–328.

[6]Forward, R. L. and Swigert, G. J., "Electronic Damping of Orthogonal Bending Modes in a Cylindrical Mast—Theory," *Journal of Spacecraft and Rockets*, Vol. 18, Jan.–Feb. 1981, pp. 5–10.

[7]Hanagud, S., Obal, M. W., and Meyyappa, M., "Electronic Damping Techniques and Active Vibration Control," AIAA Paper 85-0725, April 1985.

[8]Bailey, T. L. and Hubbard, J. E., "Distributed Piezoelectric-Polymer Active Vibration Control of a Cantilever Beam," *Journal of Guidance, Control, and Dynamics*, Vol. 8, Sept.–Oct. 1985, pp. 605–611.

[9]Gallantree, H. R. and Quilliam, R. M., "Polarized Poly (Vinylidene Fluoride)—Its Application to Pyroelectric and Piezoelectric Devices," *The Marconi Review*, Fourth Quarter, 1976, pp. 189–200.

[10]Kagawa, Y. and Gladwell, G. M. N., "Finite Element Analysis of Flexure-type Vibrations with Electrostrictive Transducers," *Transactions on Sonics and Ultrasonics*, Vol. SU-17, No. 1, Jan. 1970, pp. 41–49.

[11]Grimes, G. C. and Adams, D. F., "Investigation of Compression Fatigue Properties of Advanced Composites," Northrop Corporation Aircraft Group, Hawthorne, CA, Tech. Rept. NOR 79-17, Oct. 1979.

[12]Meirovitch, L., *Elements of Vibration Analysis*, McGraw-Hill, New York, 1975.

[13]Tsai, S. W. and Hahn, H. T., *Introduction to Composite Materials*, Technomic Publishing Co., Stamford, CT, 1980.